Novel Ruthenium–Oxo Complexes of Saturated Macrocycles with Nitrogen and Oxygen Donors and X-ray Crystal Structure of *trans*-$[Ru^{IV}(L)O(H_2O)][ClO_4]_2$

Chi-Ming Che,* Wai-Tong Tang, Wing-Tak Wong, and Ting-Fong Lai†

Contribution from the Department of Chemistry, University of Hong Kong, Pokfulam Road, Hong Kong. *Received November 7, 1988*

Abstract: Reaction of $K_2[RuCl_5(H_2O)]$ with L (1,12-dimethyl-3,4:9,10-dibenzo-1,12-diaza-5,8-dioxacyclopentadecane) in refluxing ethanol yielded *trans*-$[Ru^{III}(L)Cl_2]^{2+}$, isolated as chloride salt. Treatment of *trans*-$[Ru^{III}(L)Cl_2]^+$ with Ag^+ in water led to the formation of *trans*-$[Ru^{III}(L)(OH)(H_2O)]^{2+}$, which could be oxidized to *trans*-$[Ru^{IV}(L)O(H_2O)]^{2+}$ and *trans*-$[Ru^{VI}(L)(O)_2]^{2+}$ by electrochemical and Ce(IV) oxidation, respectively. Magnetic susceptibility measurements on the perchlorate salts of *trans*-$[Ru^{III}(L)(OH)(H_2O)]^{2+}$, *trans*-$[Ru^{IV}(L)(O)(H_2O)]^{2+}$, and *trans*-$[Ru^{VI}(L)(O)_2]^{2+}$ showed that their μ_{eff} values are 1.86, 2.87, and 0 μ_B, respectively, in accordance to their electronic formulation [Ru(III), $(d_{xy})^2(d_{xz} + d_{yz})^2(d_{xz} - d_{yz})^1$; Ru(IV), $(d_{xy})^2(d_{xz})^1(d_{yz})^1$; Ru(VI), $(d_{xy})^2$]. The Ru=O stretching frequencies for the Ru(IV) and Ru(VI) complexes are 845 and 865 cm^{-1}. The X-ray crystal structure of *trans*-$[Ru^{IV}(L)(O)(H_2O)][ClO_4]_2 \cdot 2H_2O$ has been determined: $C_{21}H_{34}N_2Cl_2O_{14}Ru$; M_r 710.47; triclinic, space group $P\bar{1}$; a = 11.157 (5), b = 11.697 (3), c = 12.598 (2) Å; α = 74.05 (1), β = 61.55 (2), γ = 71.33 (2)°; V 1354.7 Å^3; Z = 2; d_{calcd} = 1.742, d_{measd} = 1.72 g cm^{-3}; μ(MO Kα) = 8.4 cm^{-1}. The coordinated oxo and aquo groups are trans to each other. The measured Ru=O distance of 1.739 (2) Å is the shortest one ever reported for oxoruthenium(IV) complexes. The intermolecular separation of two Ru=O moieties is 2.8 Å, which features significant nonbonded [Ru=O···O=Ru] interaction. At pH = 1.1, the $E_{1/2}$ values for the *trans*-$[Ru^{VI}(L)(O)_2]^{2+}$/*trans*-$[Ru^{IV}(L)(O)(H_2O)]^{2+}$ and *trans*-$[Ru^{IV}(L)O(H_2O)]^{2+}$/*trans*-$[Ru^{III}(L)(OH)(H_2O)]^{2+}$ couples are, respectively, 0.92 and 0.58 V vs SCE. Thus, *trans*-$[Ru^{VI}(L)(O)_2]^{2+}$ is a powerful oxidant and is 0.26 V more oxidizing than *trans*-$[Ru^{VI}(TMC)(O)_2]^{2+}$ (TMC = 1,4,8,11-tetramethyl-1,4,8,11-tetraazacyclotetradecane). *trans*-$[Ru^{VI}(L)(O)_2]^{2+}$ is capable of oxidizing a wide variety of organic substrates, including alcohols, olefins, aromatic hydrocarbons, and adamantane under mild conditions. Electrocatalytic oxidation of benzyl alcohol and oxidation of organic substrates with PhIO are achieved with the $[Ru^{III}(L)(OH)(H_2O)]^{2+}$ or $[Ru^{IV}(L)(O)(H_2O)]^{2+}$ complex as catalyst.

There is a growing interest in the oxidation chemistry of ruthenium–oxo complexes,[1,2] because of their potential application in catalytic and stiochiometric oxidation of organic substrates. Our recent studies have shown that ruthenium–oxo complexes in oxidation states of IV–VI can be stabilized with macrocyclic tertiary amine ligands, such as TMC (1,4,8,11-tetramethyl-1,4,8,11-tetraazacyclotetradecane).[2c] These ruthenium macrocyclic complexes, which are stable toward demetalation, have been found to possess reversible electrochemistry[3] and provide a good model system for mechanistic investigation of proton-coupled multielectron-transfer reactions. However, except for the *trans*-$[Ru^{V}(TMC)O(X)]^{2+}$ (X = Cl, N_3, and NCO) cations, which are generated in situ by electrochemical means,[2a,f] the reported ruthenium(IV)- and ruthenium(VI)–oxo complexes of TMC are not capable of oxidizing substrates at an appreciable rate at room temperature,[2c] thus hindering their uses as oxidative catalysts.

We are concerned with the synthesis of macrocyclic ruthenium–oxo complexes with sufficiently high redox potentials for C–H bond oxidation. Also, systematic variation of the redox potentials of ruthenium–oxo complexes in a given oxidation state would lead to a new class of compounds suitable for the study of driving force dependence in organic oxidation. In this respect, our methodology involves tuning the physical properties and redox potentials of the metal complexes through variation of the structure of nonlabile equatorial ligands.[4] We describe here the generation of a new class of highly oxidizing ruthenium–oxo complexes, which effect chemical and electrochemical oxidation of organic substrates with a saturated macrocyclic ligand having nitrogen and oxygen donors, L (1,12-dimethyl-3,4:9,10-dibenzo-1,12-diaza-5,8-dioxacyclopentadecane). The structure of the novel *trans*-$[Ru^{IV}(L)O(H_2O)]^{2+}$ complex, a prototype example of *trans*-oxoaquoruthenium(IV) system, has been established by X-ray crystallography.

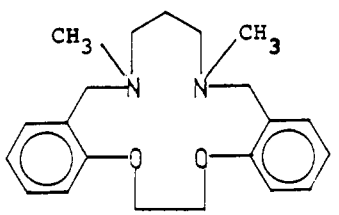

Ligand L

Experimental Section

Materials. $K_2[RuCl_5(H_2O)]$ (Johnson and Matthey) was used as received. Trifluoroacetic acid (99%, Aldrich) was purified by distillation under nitrogen atmosphere. Acetonitrile (Mallinkrodt chromAR) was purified by treatment with $KMnO_4$ and then distillation over CaH_2. Tetrabutylammonium fluoroborate (Southwestern Analytical Chemicals, electrochemetric grade) for electrochemical studies was dried in a vacuum oven at 100 °C for 24 h. The organic substrates used in oxidation were purified by standard methods, and the purity was checked by gas chromatography. The ligand, 1,12-dimethyl-3,4:9,10-dibenzo-1,12-diaza-5,8-dioxacyclopentadecane, was prepared by literature method.[5]

† Correspondence on X-ray work should be addressed to Dr. Lai.

(1) Recent works on Ru=O complexes by other researchers: (a) Roecker, L.; Meyer, T. J. *J. Am. Chem. Soc.* **19877**, *109*, 746. (b) Lau, T. C.; Kochi, J. K. *J. Chem. Soc., Chem. Commun.* **1987**, 748. (c) Griffith, W. P.; Ley, S. V.; Whitcombe, G. P.; White, A. D. *J. Chem. Soc., Chem. Commun.* **1987**, 1625. (d) El-Hendawy, A. M.; Griffith, W. P.; Piggott, B.; Williams, D. J. *J. Chem. Soc., Dalton Trans.* **1988**, 1983. (e) Marmion, M. E.; Takeuchi, K. J. *J. Am. Chem. Soc.* **1988**, *110*, 1472. (f) Llobet, A.; Doppelt, P.; Meyer, T. J. *Inorg. Chem.* **1988**, *27*, 514. (g) Bailey, C. L.; Drago, R. S. *J. Chem. Soc., Chem. Commun.* **1987**, 179. (h) Nazeeruddin, M. K.; Rotzinger, F. R.; Comte, P.; Gratzel, M. *J. Chem. Soc., Chem. Commun.* **1988**, 872.

(2) (a) Che, C. M.; Wong, K. Y.; Mak, T. C. W. *J. Chem. Soc., Chem. Commun.* **1985**, *546*, 988. (b) Che, C. M.; Wong, K. Y.; Leung, W. H.; Poon, C. K. *Inorg. Chem.* **1986**, *25*, 345. (c) Che, C. M.; Lai, T. F.; Wong, K. Y. *Inorg. Chem.* **1987**, *26*, 2289. (d) Che, C. M.; Leung, W. H. *J. Chem.* soc., *Chem. Commun.* **1987**, 1376. (e) Che, C. M.; Yam, V. W. W. *J. Am. Chem. Soc.* **1987**, *109*, 1262. (f) Wong, K. Y.; Che, C. M.; Anson, F. C. *Inorg. Chem.* **1987**, *26*, 737.

(3) (a) Che, C. M.; Wong, K. Y.; Anson, F. C. *J. Electroanal. Chem. Interfacial Electrochem.* **1987**, *226*, 211. (b) Che, C. M.; Poon, C. K. *Pure Appl. Chem.* **1988**, *60*, 1201.

(4) See also: Yam, V. W. W.; Che, C. M.; Tang, W. T. *J. Chem. Soc., Chem. Commun.* **1988**, 100.

0002-7863/89/1511-9048$01.50/0

$[Ru^{III}(L)Cl_2]Cl$. An ethanolic solution of the ligand L (1.5 mmol in 200 mL) was added dropwise to a rigorously stirred ethanolic suspension of $K_2[RuCl_5(H_2O)]$ (0.5 g, 1.4 mmol) under refluxing condition. The addition process took 3 h for completion, and the mixture was further refluxed for another 12 h. This was then filtered, and the filtrate was evaporated to nearly dryness. The orange $[Ru^{III}(L)Cl_2]Cl$ solid was precipitated upon addition of water (10 mL); yield 67%. Anal. Calcd for $[Ru(L)Cl_2]Cl$: C, 46.0; H, 5.1; N, 5.1. Found: C, 46.2; H, 5.0; N, 5.2. UV–vis [λ_{max} (ϵ) in CH_3CN]: 379 (1540), 274 (4530), 218 nm (11 900). The following three compounds are isolated as perchlorate salts. *Caution*! Perchlorates are potentially shock-sensitive and should be handled in small quantity.

***trans*-$[Ru^{III}(L)(OH)(H_2O)](ClO_4)_2 \cdot 2H_2O$.** A mixture of $[Ru^{III}(L)Cl_2]Cl$ (0.3 g) and silver(I) toluene-*p*-sulfonate (0.5 g) in distilled water (25 mL) was heated at 80 °C for 0.5 h until all the starting $[Ru^{III}(L)Cl_2]Cl$ solid had been dissolved. A greenish yellow solution was obtained. This was filtered to remove the insoluble silver chloride. The yellow *trans*-$[Ru^{III}(L)(OH)(H_2O)](ClO_4)_2$ solid was precipitated by the addition of $NaClO_4$. Crystallization was performed using hot trifluoroacetic acid (0.2 M). Yield was quantitative. Anal. Calcd for *trans*-$[Ru^{III}(L)(oH)(H_2O)](ClO_4)_2 \cdot 2H_2O$: C, 35.40; H, 4.9; N, 3.9; Cl, 9.9. Found: C, 35.4; H, 4.8; N, 3.8; Cl, 9.6. IR (Nujol mull): $\nu(H_2O)$ 3350 cm^{-1}. UV–vis [λ_{max} (ϵ) in H_2O]: 320 (1510), 275 (2680), 223 nm (7200).

***trans*-$[Ru^{IV}(L)O(H_2O)](ClO_4)_2 \cdot 2H_2O$.** This was prepared electrochemically by constant potential electrolysis of a 1 mmol solution (0.1 M CF_3COOH/CF_3COONa) of *trans*-$[Ru^{III}(L)(OH)(H_2O)](ClO_4)_2$ at a potential of 0.8 V vs SCE. The *trans*-$[Ru^{IV}(L)O(H_2O)]^{2+}$ complex was precipitated out from the solution by addition of $NaClO_4$. Yield was quantitative. Anal. Calcd for $[Ru^{IV}(L)O(OH_2)](ClO_4)_2 \cdot 2H_2O$: C, 35.5; H, 4.7; N, 3.9; Cl, 9.9. Found: C, 35.6; H, 4.7; N, 3.9; Cl, 9.8; UV–vis [λ_{max} (ϵ) in H_2O]: 540 (120), 265 (2400), 232 nm (8300).

***trans*-$[Ru^{VI}(L)(O)_2](ClO_4)_2$.** *trans*-$[Ru^{IV}(L)(OH)(H_2O)](ClO_4)_2$ (0.1 g) was dissolved in deionized water (20 mL). To the stirred solution was added excess $[NH_4]_2[Ce(NO_3)_6]$ (0.2 g). Upon standing, $[Ru^{VI}(L)(O)_2](ClO_4)_2$ gradually precipitated out as an orange solid, yield ~80%. Anal. Calcd for *trans*-$[Ru^{VI}(L)(O)_2](ClO_4)_2$: C, 37.5; H, 4.2; N, 4.2; Cl, 10.5. Found: C, 37.2; H, 4.3; N, 4.0; Cl, 10.4. UV–vis [λ_{max} (ϵ) in H_2O]: 385 (2510), 230 nm (8400). IR (Nujol mull): $\nu_{as}(RuO_2)$ 865 cm^{-1}.

Physical Measurements. Elemental analyses of the newly prepared complexes were performed by Butterworth Laboratories Ltd. IR spectra were measurd in Nujol mull using Perkin Elmer 577 spectrophotometer (4000–200 cm^{-1}). Electronic absorption spectra of freshly prepared solutions were measured with a Shimadzu UV240 spectrophotometer. Magnetic susceptibilities of solid samples were measured at room temperature by the Guoy method using mercury tetrathiocyanatocobaltate(II) as the calibrant.

Cyclic voltammograms were obtained with Princeton Research (PAR) instruments model 175 (universal programmer) and model 173 (potentiostat–galvanostat). Working electrodes are pyrolytic graphite and glassy carbon. Before each cyclic voltammetric scan, the electrodes were pretreated by procedures as described previously.[3] Saturated calomel electrode (SCE) was used as the reference electrode.

Controlled potential coulometry was performed using a PAR Model 377A coulometric cell and a PAR Model 179 digital coulometer. The working electrode was a glassy-carbon cup (Atomergic Chemical V25-12).

Catalytic reactions between the ruthenium complexes and various organic substrates (0.3 mmol) in the presence of iodosylbenzene (0.2 mmol) were performed by dissolving both the ruthenium complex (0.002 mmol) and substrate in acetonitrile (2 mL). Stoichiometric oxidation of organic substrates by *trans*-$[Ru^{VI}(L)(O)_2](ClO_4)_2$ was performed by dissolving the ruthenium(VI) complex (0.05 mmol) in acetonitrile (1 mL) containing the dissolved substrate (0.5 mmol). The reaction mixture was stirred with a magnetic stirrer under degassed and dark conditions and the temperature maintained at room temperature in a water bath. Controlled experiment in the absence of the ruthenium complex was performed for each reaction. The products were analyzed by gas chromatography, ^1H NMR, mass spectrometry, and UV–visible spectroscopy.

Gas chromatographic analyses were conducted using a Varian model 940 gas chromatograph with flame ionization detector. Gas chromatographic columns used include a 10% w/w Carbowax 20M on Chromosorb W (80–100 mesh size), $^1/_8$ in. × 6 ft stainless steel column, a 10% w/w SE-30 on Chromosorb W (80–100 mesh size), $^1/_8$ in. × 6 ft stainless steel column, with nitrogen as the carrier gas. Component identification was established by comparing the retention time with authentic sample and by gas chromatographic–mass spectral analysis (GC–MS). Quantitation of individual gas chromatographic components was performed by the internal standard method employing a Shimadzu C-R3A electronic integrator. *cis*- and *trans*-stilbene oxides were quantified by ^1H NMR spectroscopy using deoxybenzoin as the internal standard. Kinetic measurements on the oxidation of organic substrates by *trans*-$[Ru^{VI}(L)(O)_2][ClO_4]_2$ were carried out spectrophotometrically with a Unicam SP8000 spectrophotometer. The reaction temperature was maintained at ±0.1 °C by circulating water through the cell holder using a Lauda Model WB-20/R thermostat bath and circulator. The reaction was followed by monitoring the decrease in absorbance of the Ru(VI) complex at 385 nm. The pseudo-first-order rate constant k_{obs} was determined from the plot of $-\ln (A - A_\infty)$ against time, where A is the absorbance at λ_{max} of the reactant complex and A_∞ is the experimentally determined infinity point. The pK_a measurements were performed using spectrophotometric method.

Table I. Crystallographic Data for $[Ru(L)(O)(H_2O)](ClO_4)_2 \cdot 2H_2O$

$[Ru(N_2O_2)O(H_2O)](ClO_4)_2 \cdot 2H_2O$	formula wt 710.47
a = 11.157 (5) Å	space group $P\bar{1}$
b = 11.697 (3) Å	T = 294 ± 1 K
c = 12.598 (2) Å	λ = 0.710 73 Å
α = 74.05 (1)°	ρ_{calcd} = 1.742 g cm^{-3}
β = 61.55 (2)°	ρ_{measd} = 1.72 g cm^{-3}
γ = 71.33 (2)°	μ = 8.4 cm^{-1}
V = 1354.7 (8) Å^3	$R(F_o)$ = 0.033
Z = 2	$R_w(F_o)$ = 0.044

X-ray Crystal Structure of $[Ru(C_{21}H_{28}N_2O_2)(O)(H_2O)](ClO_4)_2 \cdot 2H_2O$. X-ray diffraction data were collected on an Enraf-Nonius CAD4 diffractometer with graphite-monochromated Mo Kα radiation (λ = 0.71073 Å). The unit cell dimensions were obtained from a least-squares fit of 25 reflections in the range of $19° < 2\theta < 25°$. The data were corrected for Lorentz and polarization effects, but no absorption correction was made. Three check reflections, monitored every 2 h, showed no significant variation in intensity. Crystal and structure determination data are summarized in Table I. Calculations were carried out on a MicroVax II computer using the Enraf-Nonius SDP programs.[6]

The position of the ruthenium atom was obtained from a Patterson synthesis, and the rest of the non-hydrogen atoms were recovered from a subsequent Fourier map. After several cycles of full-matrix least-squares refinement, the hydrogen atoms were revealed in a difference Fourier map; however, in the structure factor calculation, only the hydrogen atoms of the water molecules were taken from the difference map while all the others were generated geometrically (C–H = 0.95 Å). All non-hydrogen atoms were refined anisotropically, and the hydrogen atoms with assigned isotropic thermal factors were not refined.

Final agreement factors are shown in Table I. Atomic coordinates of non-hydrogen atoms are listed in Table II. Selected bond distances and angles are given in Table III. Tables of hydrogen atomic parameters, anisotropic thermal parameters, some distances and angles, some least-squares planes, and structure factors are available as supplementary material.

Results and Discussion

The ligand L, a saturated macrocycle having nitrogen and oxygen donors, was previously reported by Lindoy and co-workers.[5] So far, its coordination chemistry is mainly confined to the complexes of first-row transition metals.[5,7] When compared to the N_4-donor macrocycles such as TMC, it has a weaker ligand field strength [10*Dq* for TMC and N_2O_2 are 11 300[8] and 9615 cm^{-1},[5a] respectively]. While it reacts with $K_2[RuCl_5(H_2O)]$ to give $[Ru(L)Cl_2]^+$ in reasonable yield, an attempt to synthesize *trans*-$[Os^{III}(L)Cl_2]^+$ following a similar procedure as that for *trans*-$[Os^{III}(TMC)Cl_2]^+$ was unsuccessful. Because of the hydrophobic nature of the two benzene rings, its metal complexes have low solubilities in water. For this reason, isolation of the perchlorate salts of *trans*-$[Ru^{III}(L)(OH)(H_2O)]^{2+}$ (**1**) and

(5) (a) Armstrong, L. G.; Grimsley, P. G.; Lindoy, L. F.; Lip, H. C.; Morris, V. A.; Smith, R. J. *Inorg. Chem.* **1978**, *17*, 2350. (b) Adam, K. R.; Anderegg, G.; Lindoy, L. F.; Lip, H. C.; McPartlin, M.; Rea, J. H.; Smith, R. J.; Tasker, P. A. *Inorg. Chem.* **1980**, *19*, 2956. (c) Ekstrom, A.; Lindoy, L. F.; Lip, C. H.; Smith, R. J.; Goodwin, H. J.; McPartlin, M.; Tasker, P. A. *J. Chem. Soc., Dalton Trans.* **1979**, 1027.

(6) Frenz, B. A. *Enraf-Nonius Structure Determination Package SDP User Guide*; Enraf-Nonius: Delft, The Netherlands, 1985.

(7) (a) Adam, K. R.; Lindoy, L. F.; Smith, R. J. *J. Chem. Soc., Chem. Commun.* **1979**, 812. (b) Goodwin, H. J.; Henrick, K.; Lindoy, L. F.; McPartlin, M.; Tasker, P. A. *Inorg. Chem.* **1982**, *21*, 3261.

(8) Wagner, F.; Barefield, E. K. *Inorg. Chem.* **1976**, *15*, 408.

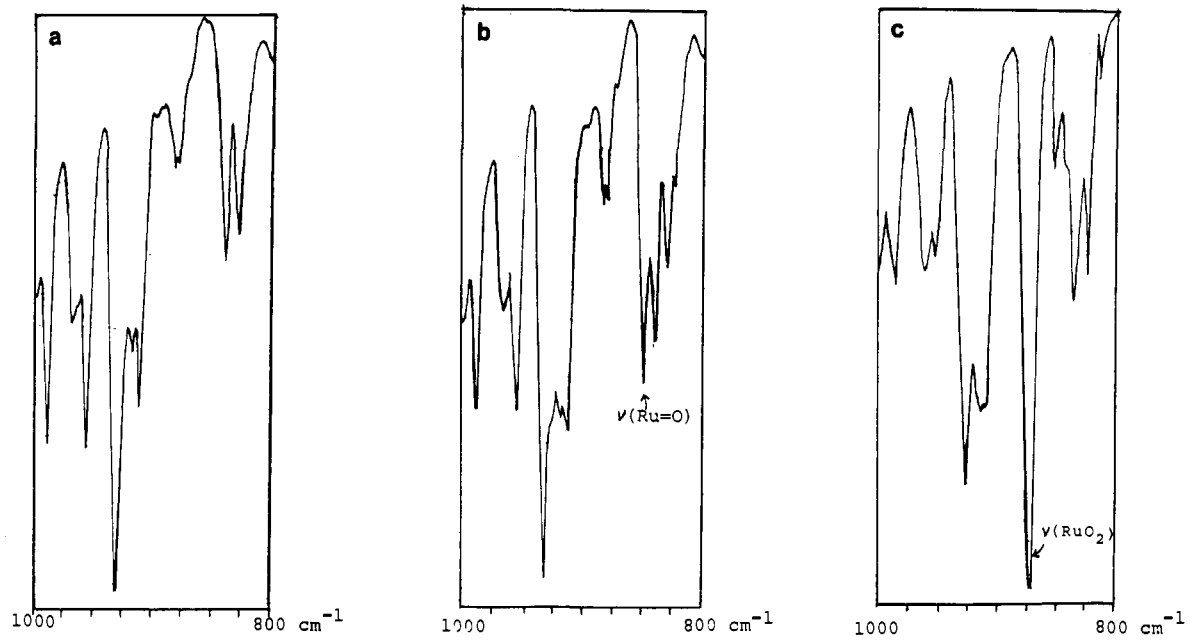

Figure 1. IR spectra of (a) **1**, (b) **2**, and (c) **3** in the 800–1000-cm^{-1} region.

Table II. Fractional Coordinates and Thermal Parameters[a] of Non-Hydrogen Atoms and Their ESD's for $[Ru(C_{21}H_{28}N_2O_2)(O)(H_2O)](ClO_4)_2 \cdot 2H_2O$

atom	x	y	z	B_{eq}, Å^2
Ru	0.12577 (2)	0.31727 (2)	0.32617 (2)	1.943 (4)
Cl(1)	0.23190 (9)	−0.1600 (1)	0.88023 (8)	4.34 (2)
Cl(2)	0.41335 (8)	0.18778 (8)	0.66170 (7)	3.68 (2)
O	0.0805 (2)	0.3911 (2)	0.4469 ((2)	2.59 (5)
O(1)	0.1570 (2)	0.1457 (2)	0.4329 (2)	2.65 (5)
O(2)	0.3414 (2)	0.2940 (2)	0.2878 (2)	2.74 (5)
O(3)	0.2093 (2)	0.2070 (2)	0.1798 (2)	3.24 (5)
O(4)	0.1466 (3)	0.2103 (5)	0.0004 (3)	6.16 (8)
O(5)	0.4775 (3)	0.0801 (4)	0.0901 (3)	7.4 (1)
O(11)	0.2667 (3)	−0.1516 (3)	0.7544 (3)	5.65 (9)
O(12)	0.1766 (5)	−0.0397 (4)	0.9125 (3)	8.9 (1)
O(13)	0.1345 (4)	−0.2313 (4)	0.9541 (4)	10.6 (1)
O(14)	0.3541 (3)	−0.2087 (4)	0.9007 (3)	7.1 (1)
O(21)	0.4163 (3)	0.0847 (3)	0.6230 (3)	5.53 (8)
O(22)	0.4240 (3)	0.1537 (3)	0.7756 (3)	6.59 (9)
O(23)	0.5302 (4)	0.2358 (4)	0.5738 (3)	8.2 (1)
O(24)	0.2896 (4)	0.2743 (4)	0.6725 (4)	9.1 (1)
N(1)	0.1237 (2)	0.4779 (2)	0.2014 (2)	2.45 (6)
N(2)	−0.0828 (2)	0.3134 (2)	0.3796 (2)	2.27 (5)
C(1)	−0.0799 (3)	0.1456 (3)	0.5546 (3)	2.60 (7)
C(2)	−0.1901 (3)	0.1301 (3)	0.6670 (3)	3.43 (9)
C(3)	−0.1705 (4)	0.0963 (4)	0.7731 (3)	4.1 (1)
C(4)	−0.0393 (4)	0.0796 (3)	0.7666 (3)	3.89 (9)
C(5)	0.0731 (3)	0.0956 (3)	0.6553 (3)	3.22 (8)
C(6)	0.0508 (3)	0.1269 (3)	0.5520 (3)	2.54 (7)
C(7)	0.3051 (3)	0.1014 (3)	0.4070 (3)	3.41 (8)
C(8)	0.3664 (3)	0.2038 (3)	0.3864 (6)	3.35 (8)
C(9)	0.3913 (3)	0.4005 (3)	0.2580 (3)	2.88 (7)
C(10)	0.4670 (3)	0.4140 (3)	0.3126 (3)	3.50 (8)
C(11)	0.5142 (3)	0.5218 (4)	0.2760 (4)	4.23 (9)
C(12)	0.4852 (4)	0.6115 (3)	0.1911 (4)	4.3 (1)
C(13)	0.4069 (4)	0.5967 (3)	0.1387 (3)	3.73 (9)
C(14)	0.3593 (3)	0.4909 (3)	0.1712 (3)	3.00 (8)
C(15)	0.2742 (3)	0.4775 (3)	0.1136 (3)	2.91 (8)
C(16)	0.0599 (3)	0.5933 (3)	0.2572 (3)	2.94 (7)
C(17)	0.0513 (3)	0.4804 (3)	0.1252 (3)	3.02 (7)
C(18)	−0.0985 (3)	0.4648 (3)	0.1980 (3)	3.17 (7)
C(19)	−0.1166 (3)	0.3411 (3)	0.2721 (3)	2.86 (7)
C(20)	−0.1889 (3)	0.3973 (3)	0.4698 (3)	2.87 (7)
C(21)	−0.0982 (3)	0.1840 (3)	0.4384 (3)	2.70 (7)

[a] Anistropically refined atoms are given in the form of the isotropic equivalent displacement parameter defined as $B_{eq} = {}^4/_3[\sum_i \sum_j \beta_{ij} \mathbf{a}_i \cdot \mathbf{a}_j]$.

trans-$[Ru^{IV}(L)(O)(H_2O)]^{2+}$ (**2**) from aqueous medium becomes feasible. Oxidation of *trans*-$[Ru^{III}(L)(OH)(H_2O)]^{2+}$ by Ce(IV) gave *trans*-$[Ru^{VI}(L)(O)_2]^{2+}$ (**3**) in quantitative yield. H_2O_2 has also been found to effect the oxidation; however, the oxidized Ru(VI) product prepared by this way is usually contaminated with some unknown species, which are difficult to remove. *trans*-$[Ru^{IV}(L)(O)(H_2O)]^{2+}$ can be most conveniently prepared in pure form by electrochemical oxidation of its Ru(III) precursor at a potential of 50 mV more positive than the $E_{1/2}$ of the Ru(IV)/Ru(III) couple.

Table III. Selected Bond Lengths and Angles with ESD's in Parentheses

	Bond Lengths, Å		
Ru–O	1.739 (2)	Ru–O(3)	2.199 (3)
Ru–O(1)	2.115 (2)	Ru–N(1)	2.094 (2)
Ru–O(2)	2.153 (2)	Ru–N (2)	2.103 (3)
	Angles, deg		
O–Ru–O(1)	90.6 (1)	O(1)–Ru–N(2)	91.2 (1)
O–Ru–O(2)	87.6 (1)	O(2)–Ru–O(3)	85.3 (1)
O–Ru–O(3)	171.4 (1)	O(2)–Ru–N(1)	93.6 (1)
O–Ru–N(1)	94.6 (2)	O(2)–Ru–N(2)	171.3 (1)
O–Ru–N(2)	92.9 (2)	O(3)–Ru–N(1)	90.6 (1)
O(1)–Ru–O(2)	80.1 (1)	O(3)–Ru–N(2)	93.4 (2)
O(1)–Ru–O(3)	83.5 (1)	N(1)–Ru–N(2)	95.1 (1)
O(1)–Ru–N(1)	171.7 (1)		

The newly prepared ruthenium complexes are air-stable solids. The dioxoruthenium(VI) complex is diamagnetic as expected for d^2 dioxometal complexes.[8,9] The measured room-temperature μ_{eff} values for the Ru(III) and Ru(IV) complexes are 1.86–1.90 and 2.87 μ_B, respectively, corresponding to the spin-only values of one and two unpaired electrons [Ru(III), $(d_{xy})^2(d_{xz} + d_{yz})^2(d_{xz} - d_{yz})^2$; Ru(IV), $(d_{xy})^2(d_{xz})^1(d_{yz})^1$]. Similar μ_{eff} values of other oxoruthenium(IV) complexes have been reported previously.[2c] The trans configurations of **1** and **3** are inferred from the X-ray crystal structure of *trans*-$[Ru^{IV}(L)(O)(H_2O)]^{2+}$ (**2**), since these three complex cations are rapidly interconverted into each other by electrochemical oxidation and reduction in aqueous solutions. For $[Ru^{III}(L)Cl_2]^+$, its UV–vis spectrum shows only one intense $p_\pi(Cl) \rightarrow d_\pi(Ru)$ charge-transfer band at 380 nm, which is characteristic of the *trans*-dichlorotetraammineruthenium(III) system.[10] A direct comparison of the IR spectra of the ruthenium(III), ruthenium(IV), and ruthenium(VI) complexes allows the identifi-

(9) See also: Griffith, W. P.; Pawson, D. *J. Chem. Soc., Dalton Trans.* **1973**, 1315.
(10) Walker, D. D.; Taube, H. *Inorg. Chem.* **1980**, *20*, 2828.

cation of Ru=O stretches, as illustrated in Figure 1. The respective $\nu_{as}(Ru^{VI}O_2)$ and $\nu(Ru^{IV}=O)$ stretches at 865 and 845 cm^{-1} are higher than those values found for the Ru(TMC)(O) analogues, *trans*-$[Ru^{VI}(TMC)(O)_2]^{2+}$, 850 cm^{-1}; *trans*-$[Ru^{IV}(TMC)(O)(X)]^{n+}$, 810–790 cm^{-1}),[2c] indicating stronger metal–oxo bonds in the present system. In fact, the Ru=O stretching frequency of complex **2** is the highest when compared to those values of 790–810 cm^{-1} found in other Ru^{IV}=O complexes.[1e,2c,11] This is also in agreement with the X-ray result as described in the following section.

The UV–vis absorption spectra of complexes **1–3** in 0.1 M CF_3SO_3H are shown in parts a–c of Figure 2. Since the optical spectra of complex **2** in acetone, water, and perchloric acid (0.1 M) are the same, the metal complex retains the (Ru=O) moiety in aqueous solutions, and the equilibrium constant for the reaction, *trans*-$[Ru^{IV}(L)(O)(H_2O)]^{2+} \rightleftharpoons$ *trans*-$[Ru^{IV}(L)(OH)_2]^{2+}$, if it exists, should be very small. The spectrum of **1** in the 300–500-nm region is similar to that for *trans*-$[Ru^{III}(bpy)_2(OH)(H_2O)]^{2+}$, showing one broad peak at 320 nm, which is assigned to the $p_\pi(OH) \rightarrow d_\pi(Ru)$ charge-transfer transition. For the monooxoruthenium(IV) system, the allowed $p_\pi(O) \rightarrow d_\pi^*$ ($d_\pi^* = d_{xy}$, d_{yz}) charge-transfer band is expected.[2c] In the case of **2**, this band probably occurs at 300–260 nm; however, the assignment is complicated by the intraligand $\pi \rightarrow \pi^*$ transition of the benzene rings in L, which also occurs in the high UV region. In Figure 2b, there is a weak absorption peak at 542 nm. The ϵ_{max} of this band is low (ca. 150 mol^{-1} dm^3 cm^{-1}), suggesting that it is probably due to the low-energy $d_{xy} \rightarrow d_\pi^*$ transition band.

In previous works,[2b,2c] it has been found that *trans*-dioxoruthenium(VI) complexes of neutral amines show characteristic vibronic structured $(d_{xy})^2 \rightarrow (d_{xy})^1(d_\pi^*)^1$ transitions at 380–400 nm. In the present Ru(VI) complex, there is also an absorption peak at 385 nm (Figure 2c), but this is unlikely to be a d–d band because of its large ϵ_{max} of 2510 mol^{-1} dm^3 cm^{-1}. It is likely that the $(d_{xy})^2 \rightarrow (d_{xy})^1(d_\pi^*)^1$ transition sits underneath some low-energy charge-transfer bands, and further spectroscopic studies are necessary before any definitive assignment can be drawn.

Complexes **1** and **2** show average pK_a values of 5.3 ± 0.3 and 5.4 ± 0.3, respectively, using spectrophotometric method. Parts a and b of Figure 3 show the optical spectra of the two independent wavelengths, and the results obtained are in good agreement with each other. The similar pK_a values of **1** and **2** are in accordance with the electrochemical work (described in the later section) where the plot of $E_{1/2}$ versus pH for the Ru(IV)/Ru(III) couple is linear with a slope of 58 mV/pH unit from pH 1 to 7. They are also significantly low compared to the pK_a value of 10.2 for $[Ru^{II}(bpy)_2(py)(OH_2)]^{2+}$ (py = pyridine), which is also a dipositive cation.[11b] The result is not unexpected given the fact that $p_\pi(OH_2)$ and $d_\pi^*(Ru)$ π-bonding interaction, which will lower the pK_a value of the coordinated H_2O, is not significant in the electron-rich Ru(II) center.

Structure Description of *trans*-$[Ru^{IV}(L)O(H_2O)][ClO_4]_2 \cdot 2H_2O$. Although the structures of monooxoruthenium(IV) complexes have previously been established in several cases, there has been no definitive structural evidence for ruthenium(IV) complexes $[Ru^{IV}(O)(H_2O)]$ having both coordinated oxo and aquo groups in the trans configuration. The $[Ru^{IV}(O)(H_2O)]$ complex, which is believed to be the product resulting from two-electron reduction of *trans*-dioxoruthenium(VI) ($[Ru^{VI}(O)_2]$) or one-electron oxidation of *trans*-aquohydroxyruthenium(III) $[Ru^{III}(OH)(H_2O)]$ in aqueous solutions is difficult to distinguish from *trans*-dihydroxyruthenium(IV) ($[Ru^{IV}(OH)_2]$) by ordinary electrochemical means, as both the $[Ru^{IV}(O)(H_2O)]$ and $[Ru^{IV}(OH)_2]$ complexes should have the same pH dependence of $E_{1/2}$ values.

Figure 4 shows the ORTEP plot of the *trans*-$[Ru^{IV}(L)(O)(H_2O)]^{2+}$ (**2**) cation with atomic numbering scheme. The coordinated geometry about the Ru atom is distorted octahedral with the oxo and H_2O ligands trans to each other. The Ru atom is essentially located at the center of the macrocycle with just 0.057-Å deviation from the mean plane defined by the N(1), N(2), O(1), and O(2) atoms. The configuration adopted by the macrocycle is similar to the nonmethylated N_2O_2 ligand (N_2O_2 represents 3,4:9,10-dibenzo-1,12-diaza-5,8-dioxacyclopentadecane) in $[Ni(N_2O_2)Cl_2]$,[5c] in which the chelate rings incorporating the

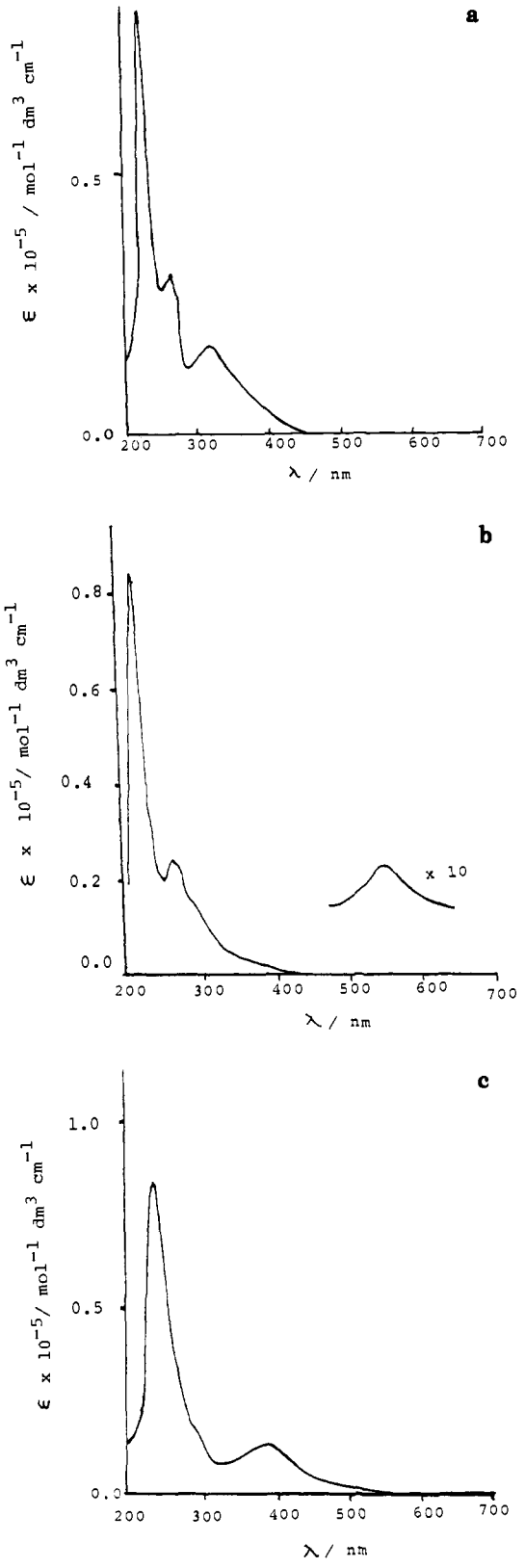

Figure 2. UV–vis absorption spectra of (a) **1**, (b) **2**, and (c) **3** in 0.1 M CF_3SO_3H.

(11) (a) Moyer, B. A.; Meyer, T. J. *J. Am. Chem. Soc.* **1978**, *100*, 3601. (b) Moyer, B. A.; Meyer, T. J. *Inorg. Chem.* **1981**, *20*, 436. (c) Roecker, L.; Kutner, W.; Gilbert, J. A.; Simmons, M.; Murray, R. W.; Meyer, T. J. *Inorg. Chem.* **1985**, *24*, 3784.

(12) For oxometal systems, the d orbitals are in the order, $d_{xy} < d_{xz},d_{yz} < d_{x^2y^2} < d_{z^2}$, after the works of Winkler Gray (*Inorg. Chem.* **1986**, *25*, 346).

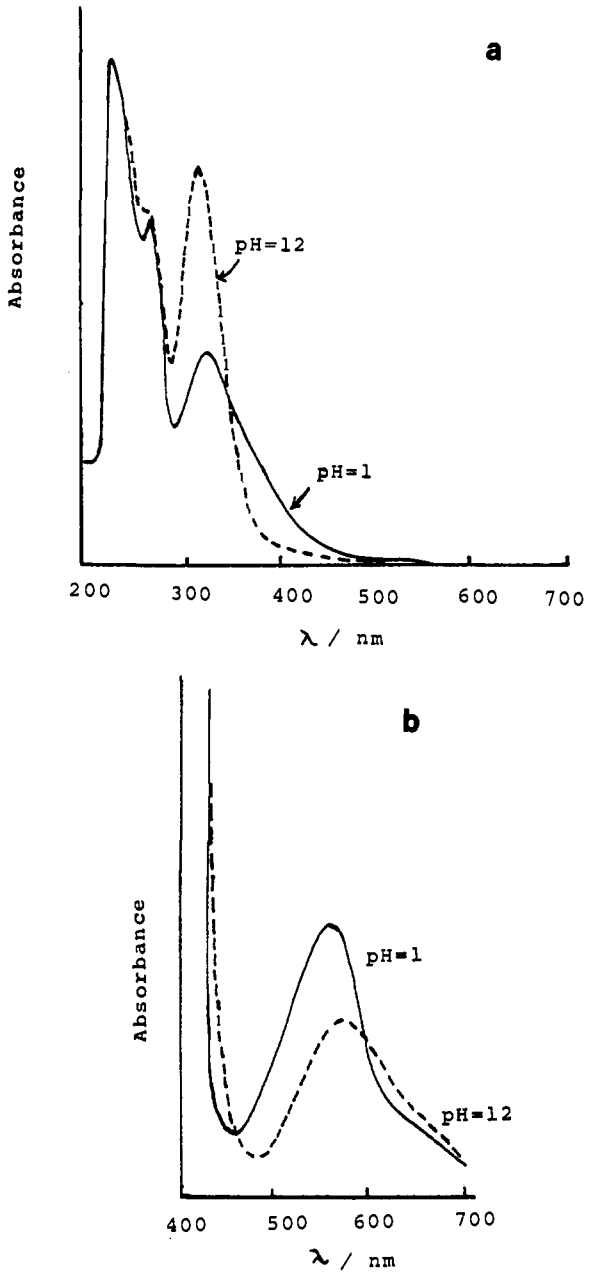

Figure 3. UV–vis absorption spectra of (a) **1** and (b) **2** at pH 1.81 and 12.0.

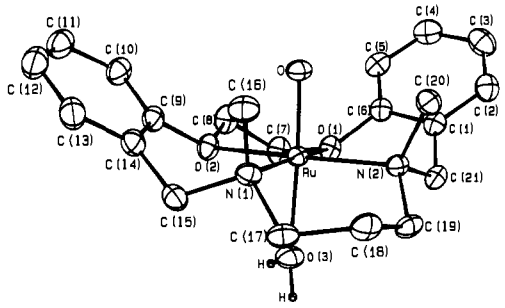

Figure 4. ORTEP plot of the *trans*-$[Ru^{IV}(L)(O)(H_2O)]^{2+}$ cation with atomic numbering scheme.

benzene rings are bent almost equally (40 and 46°) to the same side of the N_2O_2 plane and the lone pairs of nitrogen atoms are oriented syn to each other. It is probable that this represents the most stable form of this type of macrocycles. The N–CH_3 and Ru=O groups are on the same side of the macrocycle. This leads to a nonbonded repulsive interaction and hence deviation of the

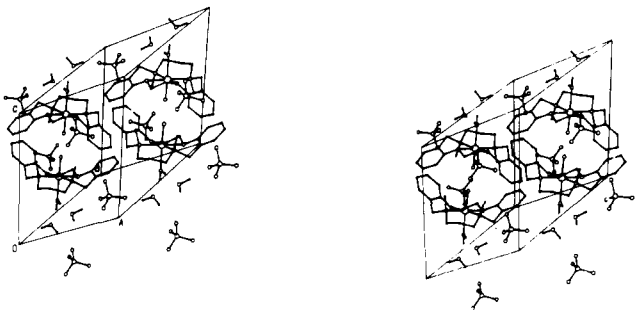

Figure 5. Stereoscopic diagram to show the packing of the *trans*-$[Ru^{IV}(L)(O)(H_2O)](ClO_4)_2$ molecules.

O–Ru–N(1) (94.6 (2)°) and O–Ru–N(2) (92.9 (2)°) angles from 90°. The coordination geometry about the nitrogen atoms is tetrahedral with the C–N–C angles (av 107.8 (5)°) expected for tertiary amines.[2c,13]

An important structural feature of the molecule is the measured Ru=O distance of 1.739 (2) Å, which is the shortest one ever reported for the oxoruthenium(IV) system. It is considerably shorter than those values in *trans*-$[Ru^{IV}(TMC)(O)(X)]^{n+}$ (1.765 (5) Å)[2c] and *trans*-$[Ru^{IV}(py)_4(O)(Cl)]^+$ (1.86 (8) Å)[14] and even comparable to the Ru=O bonds in some ruthenium(VI)–oxo complexes such as $[Ru^{VI}(bpy)(O)_2(CH_3COO)_2]$, $[Ru(O)_2(HIO_6)_2]^{6-}$, and $Ba[Ru^{VI}O_3(OH)_2]$ where the Ru=O distances are 1.726 (1),[1b] 1.732 (8),[1d] and 1.755 Å,[15] respectively. Previous work has shown that the nature of axial ligands in the *trans*-$[Ru^{IV}(TMC)(O)(X)]^{n+}$ system has no effect on the Ru=O distances.[2c] Thus the difference in the d(Ru=O) values in **2** and *trans*-$[Ru^{IV}(TMC)(O)(X)]^{n+}$ is likely due to the effect of the equatorial macrocycle. Since L is a weaker donor than TMC,[5a,8] the ruthenium ion in **2** is more electropositive, leading to an enhanced $p_\pi(O)$–$d_\pi(Ru)$ π-bonding interaction. The measured Ru–O(1) and Ru–O(2) distances of 2.115 (2) and 2.153 (2) Å are similar to the Ru–OH_2 distance of 2.136 (4) Å in $[(bpy)_2(H_2O)Ru^{III}]_2O^{4+}$ [16] but significantly longer than those values found in the structures of $[Ru(H_2O)_6]^{3+}$ (2.016 (4)–2.037 (5) Å)[17] and *trans*-$[Ru^{III}(bpy)_2(OH)(OH_2)]^{2+}$ (2.007 (3) Å). The unusual long Ru–O(3) distance of 2.199 (3) Å is probably a consequence of the trans effect of the oxo group. The Ru–N distances of 2.094 (2) and 2.103 (3) Å are comparable to those values found in the Ru–TMC system.[2a,2c]

Figure 5 shows the drawing for the crystal lattice of the Ru(IV) complex. An important structural feature of the crystal-packing diagram is that the Ru=O moieties of the *trans*-$[Ru^{IV}(L)(O)(H_2O)]^{2+}$ cations orient toward one another. Despite the fact that the close approach of two *trans*-$[Ru^{IV}(L)(O)(H_2O)]^{2+}$ cations would lead to unfavorable coulombic repulsion, the intermolecular separation of the Ru=O units is 2.85 Å, indicating the existence of [Ru=O···O=Ru] interaction, though small. Such interaction of Ru=O moieties is undoubtedly involved in the coupling reactions of ruthenium–oxo complexes and has long been suggested to be crucial for the water oxidation mediated by binuclear ruthenium complexes via

(13) Che, C. M.; Cheng, W. K.; Lai, T. F.; Poon, C. K.; Mak, T. C. W. *Inorg. Chem.* **1987**, *26*, 1678.
(14) Yukawa, Y.; Aoyagi, K.; Kurihara, M.; Shinai, K.; Shimiza, K.; Mukaida, M.; Takeuchi, T.; Kakihana, H. *Chem. Lett.* **1985**, 283.
(15) Nowogrocki, G.; Abraham, F.; Trehoux, J.; Thomas, D. *Acta Crystallogr., Sect. B* **1976**, *B32*, 2413.
(16) Gilbert, J. A.; Eggleston, D. S.; Murphy, W. R. Jr.; Gaselowitz, D. A.; Gersten, S. W.; Hodgson, D. J.; Meyer, T. J. *J. Am. Chem. Soc.* **1985**, *107*, 3855.
(17) Dong, V.; Keller, H. J.; Endress, H.; Moroni, W.; Nothe, D. *Acta Crystallogr. Sect. B.* **1977**, *B33*, 2428.
(18) Durham, B.; Wilson, S. R.; Hodgson, D. J.; Meyer, T. J. *J. Am. Chem. Soc.* **1980**, *102*, 600.
(19) Rotzinger, F. R.; Munavalli, S.; Comte, P.; Hurst, J. K.; gratzel, M.; Pern, F. J.; Frank, A. J. *J. Am. Chem. Soc.* **1987**, *109*, 6619.

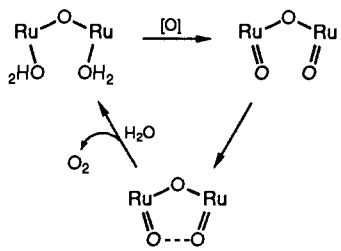

We believe that, in the highly oxidizing cationic ruthenium–oxo complexes such as **2**, the oxo groups are electrophilic and possess "oxene" character,[20] which may be responsible for the observed [Ru=O···O=Ru] interaction.

Electrochemistry. The electrochemistry of *trans*-$[Ru^{VI}(L)(O)_2]^{2+}$ (**3**) is similar to its bpy[2b] or TMC analogue.[3a] In aqueous solutions, the cyclic voltammograms of **1–3** are the same except the potentials of zero current are at different values. Three reversible/quasi-reversible couples I–III at the respective $E_{1/2}$ values of 0.26, 0.62, and 0.92 V, corresponding to the electrode reactions

$$trans\text{-}[Ru^{III}(L)(OH)(H_2O)]^{2+} + H^+ + e^- \rightarrow trans\text{-}[Ru^{II}(L)(H_2O)_2]^{2} \quad (I)$$

$$trans\text{-}[Ru^{IV}(L)(O)(H_2O)]^{2+} + H^+ + e^- \rightarrow trans\text{-}[Ru^{III}(L)(OH)(H_2O)]^{2} \quad (II)$$

$$trans\text{-}[Ru^{VI}(L)(O)_2]^{2+} + 2H^+ + 2e^- \rightarrow trans\text{-}[Ru^{IV}(L)(O)(H_2O)]^{2+} \quad (III)$$

are found at pH 1.1 as shown in Figure 6a. Controlled-potential coulometry of **1–3** in 0.1 M CF_3SO_3H with potentials held at 0.2, 0.5, and 0.7 V vs SCE established $n = 1$ for couples I and II and $n = 2$ for couple III in accordance with their formulation. For couple I, the peak to peak separation ($\Delta E_p \sim 60$ mV) and current ratio ($i_{pa}/i_{pc} = 1$) show little dependence on scan rates and electrode surfaces. For couples II and III, because the electrode reactions are accompanied with a slow proton-transfer step, their reversibilities are strongly affected by scan rates and the nature of electrode surfaces.[3a] Quasi-reversible couples are observed only with edge-plane pyrolytic graphite electrode and at scan rates of 20–100 mV s^{-1}. With glassy-carbon or platinum electrode, the couples become less reversible or irreversible. As pH is increased, couple III begins to split into two quasi-reversible one-electron couples, IV and V, appearing at 0.70 and 0.49 V, respectively, at pH 8.0 (Figure 6b). These two couples are assigned to Ru(VI)/Ru(V) and Ru(V)/Ru(IV) couples and the corresponding electrode reactions are

$$trans\text{-}[Ru^{VI}(L)(O)_2]^{2+} + e^- \rightarrow trans\text{-}[Ru^{V}(L)(O)_2]^{+} \quad (IV)$$

$$trans\text{-}[Ru^{V}(L)(O)_2]^{+} + H^+ + e^- \rightarrow trans\text{-}[Ru^{IV}(L)(O)(OH)]^{+} \quad (V)$$

When the pH of the medium is raised, the $E_{1/2}$ values of couples I–III and V (Table IV) will shift cathodically while that for couple IV remains independent of pH as expected. The plots of $E_{1/2}$ versus pH for all these couples at pH 1–8 are shown in Figure 7. Linear plots for couples III and V with slopes of −58 mV/pH unit are found in accordance with their formulations as two-proton two-electron and one-proton one-electron transfer processes, respectively. For couple II, the plot with a slope of −58 mV/pH unit is linear over the pH range of 1–8 indicative of a one-proton one-electron transfer reaction throughout this pH range. The result is not unexpected since the pK_a values for *trans*-$[Ru^{III}(L)(OH)(H_2O)]^{2+}$ and *trans*-$[Ru^{IV}(L)(O)(H_2O)]^{2+}$ are similar. In the case of couple I, there are two straight line portions with different slopes. At $1 < pH < 5.4$, the slope is −58 mV/pH unit

(20) The term "oxene" is used by Sawyer and co-workers to formulate the valency of oxygen in metal–oxo compounds. For example, see: Sawyer, T. J. *Comments Inorg. Chem.* **1987**, *6*, 103.

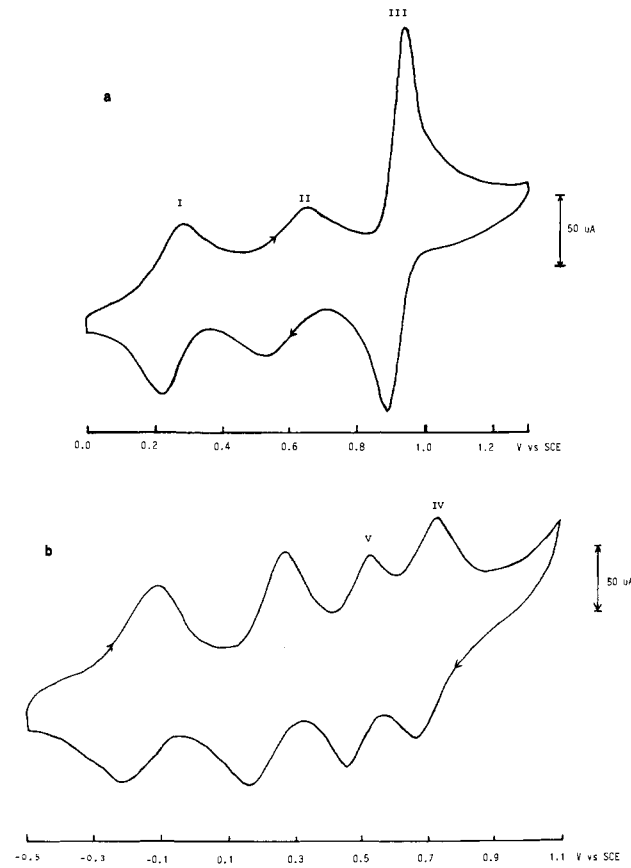

Figure 6. Cyclic voltammograms of *trans*-$[Ru^{III}(L)(OH)(H_2O)]^{2+}$ at (a) pH 1.0 and (b) pH 8.0: working electrode, pyrolytic graphite; scan rate, 50 mV s^{-1}.

Table IV. $E_{1/2}$ Values for Various Redox Couples of *trans*-$[Ru^{III}(L)(H_2O)(OH)]^{2+}$ at 25 °C

	$E_{1/2}$, V vs SCE				
pH	III/II	IV/III	V/IV	VI/IV	VI/V
1.10	0.26	0.62		0.92	
1.81	0.24	0.58		0.87	
2.21	0.22	0.55		0.85	
2.56	0.20	0.53		0.82	
3.29	0.16	0.47		0.78	
3.78	0.14	0.45		0.75	
4.10	0.11	0.43		0.73	
4.50	0.085	0.39		0.71	
5.02	0.065	0.37		0.70	
5.73	0.025	0.34		0.67	
6.37	−0.035	0.30	0.60		0.70
6.80	−0.07	0.28	0.56		0.70
7.24	−0.11	0.25	0.53		0.70
7.54	−0.14	0.22	0.51		0.70
8.00	−0.19	0.20	0.49		0.70

whereas at $pH > 5.4$, it changes to −117 mV/pH unit. On the basis of this finding, the electrode reactions are for $1 < pH < 5.4$

$$trans\text{-}[Ru^{III}(L)(OH)(H_2O)]^{2+} + e^- + H^+ \rightarrow trans\text{-}[Ru^{II}(L)(H_2O)_2]^{2+}$$

and for $5.4 < pH < 8$

$$trans\text{-}[Ru^{III}(L)(OH)_2]^{+} + e^- + 2H^+ \rightarrow trans\text{-}[Ru^{II}(L)(H_2O)_2]^{2+}$$

since, at $pH > 5.4$, the electrode reaction is a two-proton one-electron transfer process; a slope of −117 mV/pH unit is expected. The break point of the plot for couple III occurs at pH 5.4, which is logically assigned to the pK_a value of *trans*-$[Ru^{III}(L)(OH)(H_2O)]^{2+}$. This value is close to the 5.3 ± 0.2 value determined by spectrophotometric method as described in the earlier section.

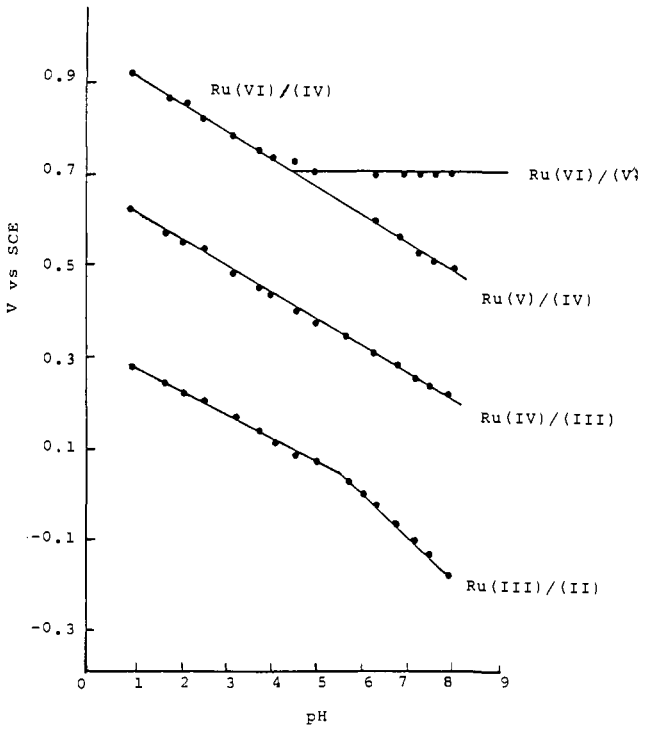

Figure 7. Plots of $E_{1/2}$ versus pH for all the redox couples of *trans*-$[Ru^{III}(L)(OH)(H_2O)]^{2+}$.

With references to previous works,[21,22] the direct two-electron reduction of **3** to **2** in acidic solutions proceeds through a Ru(V) intermediate, which is thermodynamically unstable with respect to disproportionation into Ru(VI) and Ru(IV). The disproportionation equilibrium constant, K_{disp}, for the reaction

$$2\,trans\text{-}[Ru^{V}(L)(O)_2]^{+} + 2H^{+} \rightarrow trans\text{-}[Ru^{VI}(L)(O)_2]^{2+} + trans\text{-}[Ru^{IV}(L)(O)(OH_2)]^{2+}$$

can be calculated by the equations

$$E_{1/2\,disp} = E_{1/2}(V/IV) - E_{1/2}(VI/V)$$

$$E_{1/2}(V/IV) = 2E_{1/2}(VI/IV) - E_{1/2}(VI/V)$$

where $E_{1/2}(V/IV)$, $E_{1/2}(VI/IV)$, and $E_{1/2}(VI/V)$ refer to the half-wave potentials of the respective half-cell reactions

$$trans\text{-}[Ru^{V}(L)(O)_2]^{+} + 2H^{+} + e^{-} \rightarrow trans\text{-}[Ru^{IV}(L)(O)(H_2O)]^{2+}$$

$$trans\text{-}[Ru^{VI}(L)(O)_2]^{2+} + 2H^{+} + 2e^{-} \rightarrow trans\text{-}[Ru^{IV}(L)(O)(H_2O)]^{2+}$$

$$trans\text{-}[Ru^{VI}(L)(O)_2]^{2+} + e^{-} \rightarrow trans\text{-}[Ru^{V}(L)(O)_2]^{+}$$

For the Ru(L)(O) system, $E_{1/2\,disp}$ is 0.44 V at pH 1.1 and hence K_{disp} is 2.77×10^{7} mol^{-1} dm^3 at 25 °C. Similar calculation on the Ru(TMC)(O) system gives a 0.86 V and 3.18×10^{11} mol^{-1} dm^3 for the respective $E_{1/2\,disp}$ and K_{disp} values. The much higher redox potential of *trans*-$[Ru^{VI}(L)(O)_2]^{2+}$ than that for *trans*-$[Ru^{VI}(TMC)(O)_2]^{2+}$ [$E_{1/2}°$ for Ru(VI)/Ru(IV) couple is 0.66 V vs SCE at pH 1.0] is attributed to the weaker donor strength of L. This would lead to the destabilization of the dioxoruthenium(VI) complex and hence a decrease in the K_{disp} value.

Stoichiometric and Catalytic Oxidation of Organic Substrates. We previously reported that *trans*-$[Ru^{VI}(TMC)(O)_2]^{2+}$ is a mild oxidant, and its reactions with toluene and olefins are very slow even at 50 °C.[2c] In this work, the ruthenium–oxo complexes of L demonstrate enhanced oxidative reactivities. From electrochemical experiments, complexes **2** and **3** are 0.22 and 0.26 V more oxidizing than *trans*-$[Ru^{IV}(TMC)(O)(OH_2)]^{2+}$ and *trans*-$[Ru^{VI}(TMC)(O)_2]^{2+}$. This increase in redox potential leads **3** to be a better oxidant. Addition of organic substrate such as alcohol, aldehyde, or olefin to an acetonitrile (or acetone) solution of **3** at room temperature results in the rapid reduction of Ru(VI); typical UV–vis spectral changes for the reaction with styrene at shown in Figure 8. The immediate ruthenium product in each case is Ru(IV) since its optical spectrum is similar to that of **2** in acetonitrile (or acetone) and it does not further react with the organic substrate unless with benzyl alcohol at high temperature (50 °C). Kinetic studies showed a second-order kinetics with rate = k[Ru(VI)][organic substrate] for the oxidation of organic substrates by **3**. Figure 9 shows the plots of the experimental pseudo-first-order rate constants (versus concentration of the

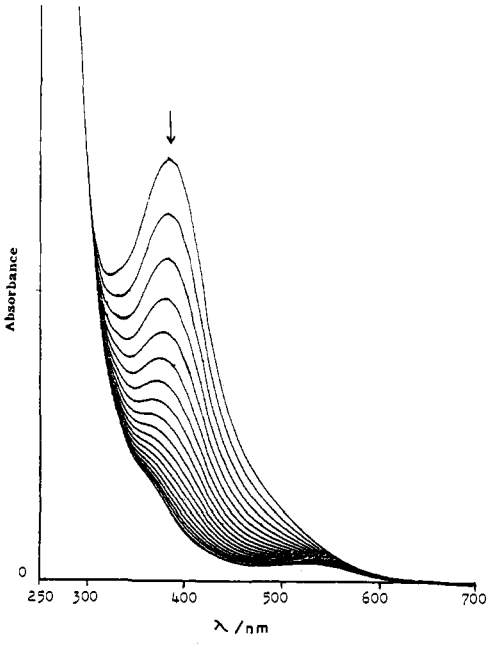

Figure 8. UV–vis spectral changes for the oxidation of styrene by *trans*-$[Ru^{VI}(L)(O)_2]^{2+}$ in CH_3CN at 298 K: scan interval, ~3 min.

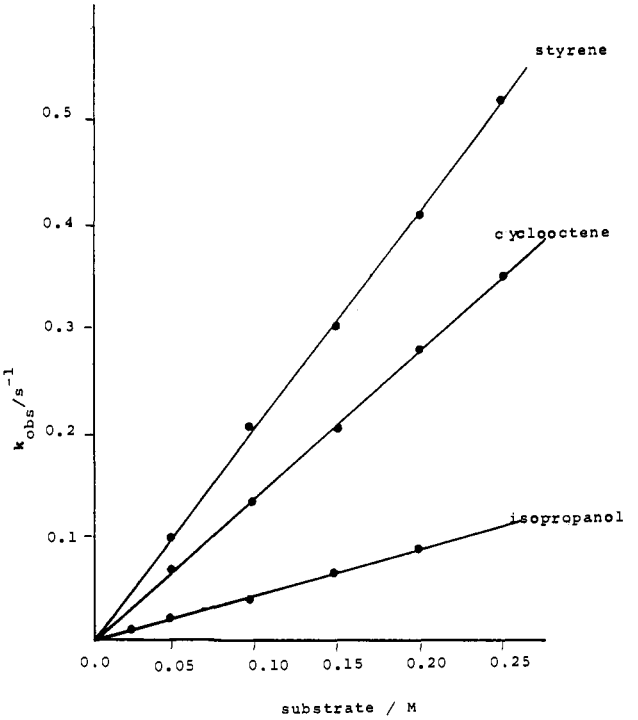

Figure 9. Plots of the experimental pseudo-first-order rate constants versus concentration of the organic substrates for the oxidative reactions of **3** in acetonitrile at 298 K.

(21) Che, C. M.; Wong, K. Y. *J. Chem. Soc., Chem. Commun.* **1986**, 229.
(22) Lau, K. Ph.D. Thesis, University of Hong Kong, 1988.

Table V. Stoichiometric Oxidation of Organic Substrates by *trans*-$[Ru^{VI}(L)(O)_2]^{2+}$ in CH_3CN at Room Temperature

substrate	product	yield,[a] %
benzyl alcohol	benzaldehyde	(100)
isopropyl alcohol	acetone	(100)
cyclohexene	cyclohexenone	(93)
cyclooctene	cyclooctene oxide	(75)
styrene	benzaldehyde	(70)
norborylene	norborylene oxide	(85)
cis-stilbene	benzaldehyde	(50)
trans-stilbene	benzaldehyde	(53)
toluene	benzaldehyde	(70)
adamantane	1-adamantanol	(50)
	2-adamantanol	(<2)
ethylbenzene	acetophenone	(61)
	sec-hphenylethyl alcohol	(37)
cumene	phenylisopropyl alcohol	(70)
tetrahydrofuran	γ-butyrolactone	(85)
cyclobutanol	cyclobutanone	(94)
cyclohexanol	cyclohexanone	(87)

Reaction time, 4 h.

Table VI. Oxidation of Organic Substrates by PhIO Catalyzed by *trans*-$[Ru^{IV}(L)(O)(H_2O)]^{2+}$ under Degassed Conditions

substrate	product	yield,[a] %
norborylene	norborylene oxide	50
styrene	benzaldehyde	30
cyclohexene	cyclohexene oxide	<3
	cyclohexen-1-ol	20
	cyclohexenone	40
cyclooctene	cyclooctene oxide	35

[a] Based on the amount of PhI produced. The reaction usually took 4–5 h when all PhIO solids were completely dissolved.

organic substrates) for the oxidation reactions of **3** in CH_3CN at 298 K. Linear plots are obtained from which the respective second-order rate constants of 0.045, 0.21, and 0.140 mol^{-1} dm^3 s^{-1} for isopropyl alcohol, styrene, and cyclooctene are deduced. The measured rate constant of 0.21 mol^{-1} dm^3 s^{-1} for the styrene oxidation is even higher than that found for oxochromium(V) salen complex [0.014–0.113 mol^{-1} dm^3 s^{-1} at 298 K under similar conditions].[23] Table V summarizes the results on the stoichiometric oxidation of organic substrate. It oxidizes alcohols to aldehydes/ketones and epoxidizes olefins. Since cyclobutanol is oxidized to cyclobutanone in quantitative yield, **3** acts as a two-electron oxidant. With styrene, oxidative cleavage of the C=C double bond is the major reaction pathway. The oxidation of cyclohexene to give cyclohexenone exclusively but with trace amount of cyclohexane oxide is similar to that found for *trans*-$[Ru^{VI}(TMC)(O)_2]^{2+}$.[2c] This suggests that **3** has a high affinity toward allylic C–H bond oxidation. It is likely that the oxo groups in *trans*-dioxoruthenium(VI) complexes of L or TMC are very electrophilic and preferentially undergo hydrogen atom/hydride abstraction rather than a concerted oxo-transfer reaction. An important finding, which suggests the potential of *trans*-dioxoruthenium(VI) in C–H bond oxidation, is that **3** can oxidize tetrahydrofuran, aromatic hydrocarbons, and adamantane to the corresponding oxidized products in high yields. Since oxidation of adamantane gives 1-adamantanol exclusively, **3** preferentially attacks a 3° C–H bond in the presence of a 2° C–H bond.

Attempts have been made to develop catalytic oxidation by reoxidation of the Ru(IV) to Ru(VI) utilizing an oxygen atom donor. The results on the oxidation of organic substrates by iodosylbenzene (PhIO) in acetone in the presence of a catalytic amount of **2** are given in Table VI. For a given substrate such as styrene, the same distribution of organic products was found in both the stoichiometric and catalytic oxidations. This suggests that the catalytic oxidation proceeded with **3** as the possible reactive intermediate. Evidence to support this suggestion comes from the finding that stirring PhIO and **2** in acetone at room temperature rapidly gave **3** as the reaction product, identified by its IR spectrum.

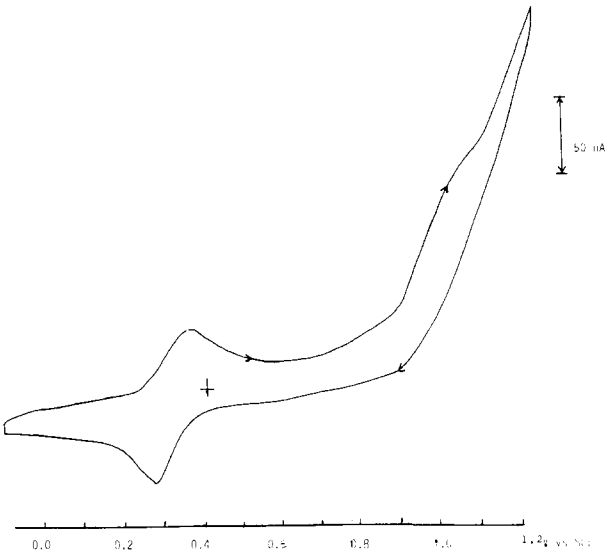

Figure 10. Cyclic voltammogram of *trans*-$[Ru^{III}(L)(OH)(H_2O)]^{2+}$ at pH 1.0 and in the presence of benzyl alcohol (0.1 M): working electrode, pyrolytic graphite; scan rate, 50 mV s^{-1}.

In view of the high redox potential of **3**, the electrocatalytic activities of its Ru(III) or (IV) precursor toward oxidation of organic substrates were tested. Figure 10 shows the cyclic voltammogram of **1** in the presence of excess benzyl alcohol. The Ru(VI)/Ru(IV) couple becomes irreversible and is replaced by an oxidative wave at potential ca. 1 V vs SCE, indicating that the electrogenerated Ru(VI) complex is rapidly reduced by benzyl alcohol under the experimental conditions. Controlled-potential electrolysis of **2** and benzyl alcohol at 1.0 V in 0.1 M CF_3SO_3H yielded benzaldehyde identified by GC–mass spectrometry. After electrolysis, the ruthenium complex remained unchanged.

Conclusion

A new class of highly oxidizing ruthenium–oxo complexes is generated with the σ-saturated macrocycle L having both nitrogen and oxygen donor atoms. The redox chemistry of the Ru(L)(O) species is similar to its TMC analogues except that the former system is more oxidizing than the latter. In fact, the $E_{1/2}$ value of complex **3** is close to that for *trans*-$[Ru^{VI}(bpy)_2(O)_2]^{2+}$ ($E_{1/2}$[Ru(VI)/Ru(IV)] is 1.01 V vs SCE),[2b] which is by far the *trans*-dioxoruthenium(VI) complex with the highest redox potential. As a consequence of this property, complex **3** shows enhanced oxidative activities. It is fairly reactive toward oxidation of alcohols and arenes and epoxidation of olefins, in contrast to *trans*-$[Ru^{VI}(TMC)(O)_2]^{2+}$ and $[Ru(bpy)(O)_2Cl_2]$,[24] which are known to be mild oxidants for oxidation of alcohols only. Given the fact that the redox potentials of ruthenium and other transition-metal macrocyclic compounds can span over a range of more than 1 V simply by changing the structure of the macrocyclic ligands,[25] it is anticipated from this study that macrocyclic dioxoruthenium(VI) complexes with different redox potentials should be easily synthesized.

Acknowledgment. We acknowledge support from the University of Hong Kong and the Croucher Foundation. W.-T.W. acknowledges the receipt of a Croucher studentship, administered by the Croucher Foundation.

Registry No. $[Ru^{III}(L)Cl_2]Cl$, 123289-03-2; $K_2[RuCl_5(H_2O)]$, 14404-33-2; *trans*-$[Ru^{II}(L)(OH)(H_2O)](ClO_4)_2$, 123265-30-5; *trans*-

(23) Samsel, E. G.; Srinivasan, K.; Kochi, J. K. *J. Am. Chem. Soc.* **1985**, *107*, 7606.

(24) Green, G.; Griffith, W. P.; Hollinshead, D. M.; Ley, S. V.; Schroder, M. *J. Chem. Soc., Perkin Trans. 1* **1984**, 681.

(25) Poon, C. K.; Kwong, S. S.; Che, C. M.; Kan, Y. P. *J. Chem. Soc., Dalton Trans.* **1982**, 1457.

$[Ru^{III}(L)O(H_2O)](ClO_4)_2 \cdot 2H_2O$, 123265-33-8; *trans*-$[Ru^{III}(L)O(H_2O)](ClO_4)_2$, 123265-32-7; *trans*-$[Ru^{VI}(L)(O)_2](ClO_4)_2$, 123265-35-0; benzyl alcohol, 100-51-6; isopropyl alcohol, 67-63-0; cyclohexene, 110-82-7; cyclooctene, 931-88-4; styrene, 100-42-5; norbornylene, 498-66-8; *cis*-stilbene, 645-49-8; *trans*-stilbene, 103-30-0; toluene, 108-88-3; adamantane, 281-23-2; ethylbenzene, 100-41-4; cumene, 98-82-8; tetrahydrofuran, 109-99-9; cyclobutanol, 2919-23-5; cyclohexanol, 108-93-0; benzaldehyde, 100-52-7; acetone, 67-64-1; cyclohexenone, 25512-62-3; cyclooctene oxide, 286-62-4; norbornylene oxide, 278-74-0; 1-adamantanol, 768-95-6; 2-adamantanol, 700-57-2; acetophenone, 98-86-2; *sec*-phenylethyl alcohol, 98-85-1; phenylisopropyl alcohol, 617-94-7; γ-butyrolactone, 96-48-0; cyclobutanone, 1191-95-3; cyclohexanone, 108-94-1; cyclohexen-1-ol, 4065-81-0; iodosylbenzene, 536-80-1.

Supplementary Material Available: Tables of anisotropic thermal parameters, hydrogen atomic parameters, bond distances and angles, least-squares planes, and experimental details for X-ray data collection (8 pages); listing of observed and calculated structure factors for $[Ru(C_{21}H_{28}N_2O_2)(O)(H_2O)](ClO_4)_2 \cdot 2H_2O$ (24 pages). Ordering information is given on any current masthead page.

Carbon Monoxide Cleavage by $(silox)_3Ta$ (silox = $^tBu_3SiO^-$): Physical, Theoretical, and Mechanistic Investigations

David R. Neithamer, Robert E. LaPointe, Ralph A. Wheeler, Darrin S. Richeson, Gregory D. Van Duyne, and Peter T. Wolczanski*,†

Contribution from the Department of Chemistry, Baker Laboratory, Cornell University, Ithaca, New York 14853. *Received March 10, 1989*

Abstract: Reduction of $(silox)_3TaCl_2$ (**1**, silox = $^tBu_3SiO^-$) with Na/Hg in THF leads to a three-coordinate, Ta(III) siloxide, $(silox)_3Ta$ (**2**). Derivatization of **2** with excess O_2 or H_2 provides $(silox)_3Ta{=}O$ (**3**) and $(silox)_3TaH_2$ (**4**), respectively. At 25 °C, carbonylation of **2** (0.1–1.0 atm) generates $^1/_2$**3** and $^1/_4[(silox)_3Ta]_2(\mu\text{-}C_2)$ (**5**), consistent with a CO uptake of 0.47 equiv. X-ray ($P\bar{1}$, R = 9.6%) structural, IR, and Raman studies of dicarbide **5** manifest a near-linear μ-C_2 bridge ($\angle$TaCC = 173 (3)°), a C=C double bond (1.37 (4) Å, ν(C=C) = 1617 cm^{-1}) and typical TaC double bonds (1.95 (2) Å, ν(Ta=C) = 709 cm^{-1}), respectively. EHMO calculations of a linear μ-C_2-bridged D_{3d} **5** indicate that the e_g^2 HOMO ($^3A_{2g}$, ^1E_g, $^1A_{1g}$) is ~80% Ta (d_{xz}, d_{yz}) and ~20% C (p_x, p_y). Magnetic susceptibility measurements of **5** from 2 to 300 K reveal a large temperature-independent susceptibility (25 °C, $\mu_{eff} = 1.93\mu_B$) and a singlet ground state, either ^1E_g, $^1A_{1g}$ (D_{3d}) or one arising from a Jahn–Teller distortion of the ^1E_g level. Treatment of **2** with CO (~1 atm) at −78 °C, followed by warming to 25 °C, results in an uptake of 0.97 equiv of CO and the production of an inseparable mixture of **3** and a monomeric ketenylidene, $(silox)_3Ta{=}C{=}C{=}O$ (**6**). Diamagnetic **6** (ν(C=O) = 2076 cm^{-1}, $^1J_{CC}$ = 100 Hz), a precursor to **5**, is linear according to EHMO calculations. Mechanistic investigations concerning formation of **5** and **6**, utilizing labeling experiments, kinetics, and chemical models, support the following sequence of reactions: (1) $(silox)_3Ta$ (**2**) binds CO to form unstable $(silox)_3TaCO$ (**2**-CO). (2) In donor solvents, **2**-CO is trapped and stabilized by the solvent (solvent = *S*) (−78 °C) as $(silox)_3STaCO$ (*S*-**2**-CO). (3) Aggregation of *S*-**2**-CO and equilibrium amounts of **2**-CO, dimerization of **2**-CO, or disproportionation of monocarbonyl species to $(silox)_3Ta(CO)_2$ (**2**-$(CO)_2$) and **2**, which quickly recombine, generates (−78 to −50 °C) red precipitate $[(silox)_3TaCO]_n$ ($[$**2**-CO$]_n$, n is probably 2). (4) In nondonor solvents **2**-CO either dimerizes or disproportionates to ultimately give $[$**2**-CO$]_n$. (5) Degradation of $[$**2**-CO$]_n$ (~5 °C), produces ketenylidene $(silox)_3Ta{=}C{=}C{=}O$ (**6**) and oxo $(silox)_3Ta{=}O$ (**3**). (6) Another $(silox)_3Ta$ (**2**) deoxygenates ketenylidene **6** (~0 °C), possibly via intermediate $(silox)_3Ta{=}C{=}\overline{C{-}O{-}Ta(silox)_3}$ (**6**·**2**), to afford oxo **3** and a transient vinylidene, $(silox)_3Ta{=}C{=}C$: (**2**-C_2), that electronically resembles CO, as substantiated by EHMO arguments. (7) A final $(silox)_3Ta$ (**2**) unit scavenges the vinylidene (**2**-C_2), resulting in $[(silox)_3Ta]_2(\mu\text{-}C_2)$ (**5**). Alternatives to the heterogeneous dissociative adsorption of CO, the first step in the Fischer–Tropsch process, are suggested on the basis of this work.

The Fischer–Tropsch (F–T) reaction,[1-4] the conversion of synthesis gas (CO/H_2) to hydrocarbons and oxygenates, has commanded the attention of the organometallic community for the past 10–15 years. During periods when olefin feedstocks are costly, the production of low molecular weight commodity chemicals from coal or natural gas via this method becomes economically attractive. The heterogeneously catalyzed F–T process is inherently nonselective since it produces a Schulz–Flory distribution of hydrocarbons, oxygenates, or both; thus homogeneous systems, considered to possess the advantage of greater selectivity, have attracted substantial interest. While a commercially feasible homogeneous F–T process has yet to be developed, some of the desired selectivity, especially toward methanol and C_2 oxygenates,[3] has been demonstrated. In addition, organometallic chemistry, through investigations of stoichiometric transformations involving carbon monoxide and dihydrogen, has dramatically increased our fundamental understanding of plausible individual steps that pertain to the F–T reaction.

The most widely accepted[4] mechanism for the heterogeneously catalyzed conversion of syngas to hydrocarbons consists of four critical steps: (1) carbon monoxide adsorbs ($(CO)_s$)[5] and dissociates on a metal surface, generating surface carbide (C_s) and oxide (O_s);[6-8] (2) surface hydrides formed upon chemisorption of di-

† Alfred P. Sloan Foundation Fellow (1987–1989).

(1) (a) Falbe, J. *Chemical Feedstocks from Coal*; John Wiley & Sons: New York, 1981. (b) Keim, W., Ed. *Catalysis in C_1 Chemistry*; D. Reidel: Dordrecht, The Netherlands, 1983. (c) Anderson, R. B. *The Fischer–Tropsch Synthesis*; Academic: New York, 1984. (d) Anderson, J. R.; Boudart, M. *Catalysis*; Springer-Verlag: Berlin, 1981; Vol. I.

(2) (a) Biloen, P.; Sachtler, W. M. H. *Adv. Catal.* **1981**, *30*, 165–216. (b) Bell, A. T. *Catal. Rev.—Sci. Eng.* **1981**, *23*, 203–232. (c) Rofer-DePoorter, C. K. *Chem. Rev.* **1981**, *81*, 447–474. (d) Masters, C. *Adv. Organomet. Chem.* **1979**, *17*, 61–103. (e) Vannice, M. A. *Catal. Rev.—Sci. Eng.* **1976**, *14*, 153–191.

(3) Dombek, B. D. *Adv. Catal.* **1983**, *32*, 325–416.

(4) (a) Fischer, F.; Tropsch, H. *Chem. Ber.* **1926**, *59*, 830–836. (b) Craxford, S. R.; Rideal, E. K. *J. Chem. Soc.* **1939**, 1604–1614.

(5) Sung, S.-S.; Hoffmann, R. *J. Am. Chem. Soc.* **1985**, *107*, 578–854, and references therein.

(6) (a) Low, G. G.; Bell, A. T. *J. Catal.* **1979**, *57*, 397–405. (b) Roberts, M. W. *Chem. Soc. Rev.* **1977**, *6*, 373–391. (c) Brodén, G.; Rhodin, T. N.; Brucker, C.; Benbow, R.; Hurych, Z. *Surf. Sci.* **1976**, *59*, 593–611.

0002-7863/89/1511-9056$01.50/0